Title

Effect of microphase separation on the limiting current density in hybrid organic-inorganic copolymer electrolytes

Authors

Sethi, Gurmukh K

Frenck, Louise

Sawhney, Simar

et al.

Publication Date

2021-10-01

DOI

10.1016/j.ssi.2021.115702

Effect of microphase separation on the limiting current density in hybrid organic-inorganic copolymer electrolytes

Gurmukh K. Sethi[†,‡], Louise Frenck[‡], Simar Sawhney[‖], Saheli Chakraborty[⊥], Irune Villaluenga[††,‡‡,*], and Nitash P. Balsara[‖,‡,§,⊥*]

*Corresponding Authors

[†]Department of Materials Science and Engineering and [‖]Department of Chemical and Biomolecular Engineering, University of California, Berkeley, California 94720, USA

[‡]Materials Science Division, [§]Joint Center for Energy Storage Research (JCESR), and [⊥]Energy Storage and Distributed Resources Division, and [▽]Advanced Light Source, Lawrence Berkeley National Laboratory, Berkeley, California 94720, USA

[††]POLYMAT University of the Basque Country UPV/EHU, 20018 Donostia-San Sebastián, Spain, and [‡‡]Ikerbasque, Basque Foundation for Science, 48013 Bilbao, Spain

TOC.

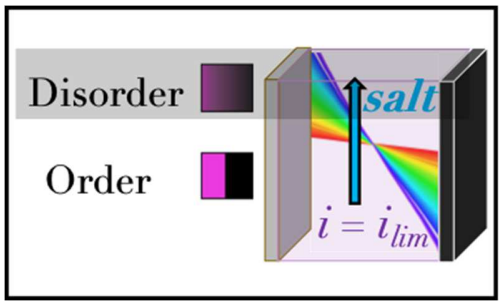

Abstract.

Hybrid organic-inorganic block copolymer electrolytes are of interest to enable batteries containing lithium metal anodes. The conductive block is a standard polymer electrolyte of poly(ethylene oxide) and the mechanically rigid block is an inorganic poly(acryloisobutyl polyhedral oligomeric silsesquioxane) polymer. In this paper, we compare a poly(acryloisobutyl polyhedral oligomeric silsesquioxane)-*b*-poly(ethylene oxide)-*b*-poly(acryloisobutyl polyhedral oligomeric silsesquioxane) (POSS-PEO-POSS) triblock copolymer and a poly(ethylene oxide)-*b*-poly(acryloisobutyl polyhedral oligomeric silsesquioxane) (PEO-POSS) diblock copolymer mixed with lithium bis(trifluoromethanesulfonyl)imide salt. We have experimentally measured the limiting current density in lithium symmetric cells containing hybrid organic-inorganic electrolytes at 90 °C. The cells were polarized at a large range of applied current density. The diblock copolymer electrolyte exhibited a clear plateau in cell potential at all current densities below the limiting current density. At low applied current density, the triblock copolymer electrolyte also exhibited a clear plateau in cell potential. At currents approaching the limiting current density, the triblock copolymer electrolyte exhibited an underdamped potential profile. The cell potential did not reach a plateau at current densities above the limiting current in both

systems. The diblock and triblock copolymer electrolytes were fully characterized using electrochemical methods to determine the ionic conductivity, cation current fraction, salt diffusion coefficient, and open circuit voltage as a function of salt concentration. Cell potential and salt concentration as functions of position in the cell at various current densities were calculated using Newman's concentrated solution theory. The theoretical limiting current density was calculated to be the current density at which salt is depleted at the cathode. We see quantitative agreement between experimental measurements and theoretical predictions for the limiting current density in the diblock copolymer electrolyte which has an ordered structure at all salt concentrations, while the experimental limiting current density is lower than the theoretical prediction for the triblock copolymer electrolyte, which exhibits a disordered morphology at high salt concentrations.

Highlights.

- Diblock copolymer electrolytes order while triblock copolymer electrolytes disorder with salt
- Predicted limiting current density is greater than experimental value in disordered system
- Predicted limiting current density agrees with experiments in ordered system

Key Words: Block copolymer electrolytes; Phase behavior; hybrid organic-inorganic; Limiting current density; Concentrated solution theory; Ion transport

Introduction. There is continued interest to develop electrolytes in order to improve stability and cycle life of secondary lithium batteries.[1–4] One approach is block copolymer electrolytes,

which combine the benefits of ionically conductive polymers with nonconducting, mechanically rigid polymers.[5] While the full electrochemical characterization of liquid electrolytes[6,7] and homopolymer electrolytes[8–10] have been extensively reported, there are relatively few systematic studies using copolymer electrolytes.[11]

Electrolytes are most often characterized by measuring ionic conductivity, κ, using ac impedance spectroscopy.[12–14] Recognizing that conductivity in Li^+ conductors is often dominated by the mobility of the anion, it is fairly common to report the cation current fraction, ρ_+, obtained in a symmetric lithium-electrolyte-lithium cell using the Bruce-Vincent method.[15,16] The product $\kappa\rho_+$ indicates the efficacy of an electrolyte in the limit of small (infinitesimal) currents.[17] Whether or not an electrolyte can be used in practical batteries depends on the relationship between current and potential in the limit of large currents.[18] While this relationship will depend on the specific battery used in the experiment, the lithium-electrolyte-lithium cell provides a standardized platform for reporting this relationship. The passage of a current through the battery results in the formation of salt concentration gradients through the electrolyte between the cathode and the anode. Salt concentration gradients in the electrolyte increase when the cell is polarized at higher current density. The limiting current density is defined as the current density at which salt is depleted at the cathode[19]. There is growing recognition that the limiting current density is, perhaps, the most important metric of an electrolyte.[20,21]

In this study we present measurements of limiting current density in a poly(acryloisobutyl polyhedral oligomeric silsesquioxane)-*b*-poly(ethylene oxide)-*b*-poly(acryloisobutyl polyhedral oligomeric silsesquioxane) (POSS-PEO-POSS) triblock copolymer and a poly(ethylene oxide)-*b*-poly(acryloisobutyl polyhedral oligomeric silsesquioxane) (PEO-POSS) diblock copolymer mixed with lithium bis(trifluoromethanesulfonyl)imide (LiTFSI) salt. In the triblock copolymer,

the PEO block has a molecular weight of 35 kg mol^{-1} and POSS block molecular weight of 4.7 kg mol^{-1}. In the diblock copolymer, the PEO block has a molecular weight of 5 kg mol^{-1} and POSS block molecular weight of 1.9 kg mol^{-1}. The volume fraction of the PEO block, f_{EO}, is 0.81 and 0.76 in triblock and diblock copolymer, respectively. Schematic 1 demonstrates the chemical structure of the diblock and triblock copolymers. The salt concentration in lithium/electrolyte/lithium cells used in the limiting current density experiments is [Li]/[EO] = r = 0.10. Table 1 summarizes the characteristics of the polymer electrolytes used in this study. The synthesis of the polymers is described in previous studies.[22,23] Block copolymers microphase separate into nanophase separated domains, creating channels that are ionically conductive. The morphology is affected by salt concentration.[24] In previous studies, we have studied this effect in a series of POSS-containing block copolymers.[22,23,25] The most commonly observed morphology in POSS-containing block copolymer/salt mixtures at 90 °C is alternating POSS-rich and PEO/LiTFSI-rich lamellae.

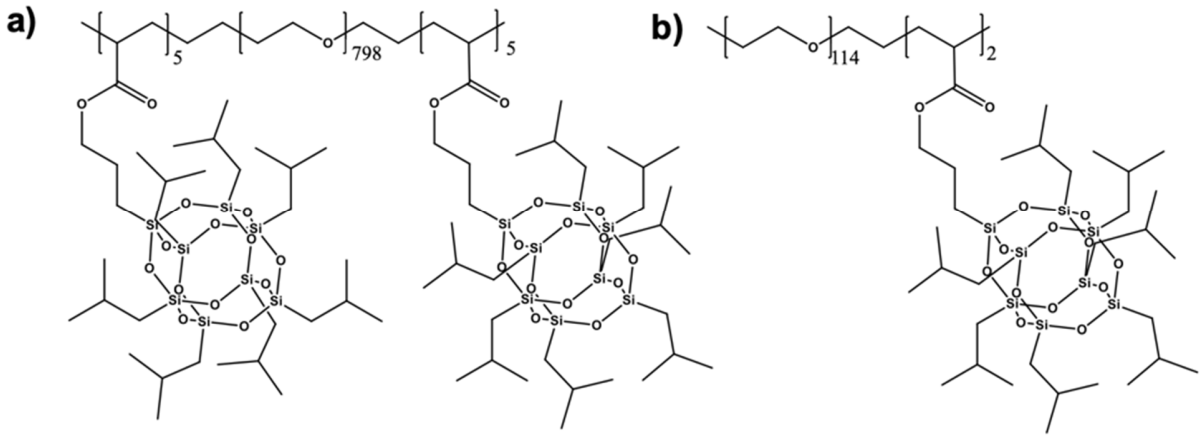

Schematic 1: Chemical structure of a) triblock copolymer (POSS-PEO-POSS) and b) diblock copolymer (PEO-POSS) used in this study.

Table 1. Characteristics of neat polymer and polymer electrolytes

	M_{PEO} (kg mol^{-1})	M_{POSS} (kg mol^{-1})	N (120 °C)	$f_{EO/LiTFSI}$	d (90 °C) (nm)	Morphology (90 °C)
Triblock $r = 0$	35	9.28	634	0.81	26.1	*LAM*
Triblock $r = 0.10$	35	9.28	634	0.85	31.4	*LAM*
Diblock $r = 0$	5	1.86	97	0.76	19.6	*LAM*
Diblock $r = 0.10$	5	1.86	97	0.80	20.0	*LAM*

M_{PEO} = molecular weight of the PEO block; M_{POSS} = molecular weight of the POSS block determined by ^{1}H-NMR; N = chain length calculated at 120 °C and monomer reference volume of 0.1 nm^3; $f_{EO/LITFSI}$ = volume fraction of PEO/LiTFSI block; d = domain spacing at 90 °C determined by small-angle X-ray scattering.

Ion transport was characterized in triblock and diblock copolymer electrolytes by experimentally measuring κ, ρ_+, salt diffusion coefficient (D), and the concentration cell open-circuit potential (U) as a function of salt concentration. Newman's concentrated solution theory can be used to model the magnitude of salt concentration gradients as a function of position in an electrolyte at different applied currents density[17]. However, this theory was developed for 3-component homogenous electrolytes. The theoretical and experimental limiting current densities in a few homogenous electrolytes has been previously reported[26–32]. In contrast, block copolymers mixed with dissociated salt are 4-component heterogenous systems and complete characterization would require specification of 6 transport parameters and 2 thermodynamic factors. A theory that incorporates these parameters has not yet been developed. Our approach

based on 3 transport coefficients and 1 thermodynamic factor is approximate. Nevertheless, this theoretical model was used to predict the limiting current density in both the triblock and diblock copolymer electrolytes. The theoretical limiting current density and the experimentally determined limiting current density are compared with no adjustable parameters.

Experimental.

Electrolyte preparation. Electrolytes were prepared by mixing polymer with LiTFSI (Sigma-Aldrich). Due to the hygroscopic nature of LiTFSI, all sample preparation was carried out in an argon glovebox (MBraun) where H_2O and O_2 levels were maintained below 0.1 ppm and 0.6 ppm respectively. PEO-POSS and POSS-PEO-POSS polymers were dried at 90 °C under vacuum in the glovebox antechamber for 48 h and then transferred into the glovebox. LiTFSI was dried at 120 °C under vacuum in the glovebox antechamber for 48 h and then transferred into the glovebox. Dry polymer and LiTFSI salt were dissolved into anhydrous THF and the solutions were mixed at 55 °C for 24 hours. The caps were then removed from the vials allowing THF to evaporate and leave behind a homogeneous polymer/salt mixture inside of the glovebox. After drying on a hotplate at 60 °C for 48 h, the electrolytes were transferred to the glovebox antechamber and dried under vacuum for 48 h at 90 °C. The salt concentration in the copolymer was quantified by r, the molar ratio of lithium ions to ethylene oxide (EO) moieties. We assume that the salt resides exclusively in the PEO domain.

Electrochemical characterization techniques.

Blocking electrode symmetric cell preparation. Stainless steel symmetric cells were prepared for ionic conductivity measurements of electrolytes using ac impedance spectroscopy. Electrolytes

were heated to 120 °C and pressed into a 3.175 mm diameter hole within a 250 μm thick silicone spacer. Two 200 μm- thick stainless-steel electrodes were pressed on either side of the electrolyte-filled spacer. The electrode thickness was measured using a micrometer. The thickness of each electrolyte (L) was determined by measuring the thickness of the cell and subtracting the thickness of the electrodes. Aluminum tabs were secured to the electrodes using Kapton tape. The entire cell was vacuum sealed in Showa-Denko pouch material leaving only the tab ends exposed.

Impedance Spectroscopy. Each cell was placed in a custom-built heating stage. Cells were held at temperature for 30 minutes before measurements were taken. Complex electrochemical impedance spectroscopy measurements were acquired using a Biologic VMP3 potentiostat paired with EC-lab software for a frequency range of 1 MHz to 100 mHz at an amplitude of 50 mV. The resulting Nyquist plot was fit to an equivalent circuit, and the electrolyte bulk resistance (R_b) was extracted. This value was identical to the R_b determined from the low-frequency minimum on a Nyquist impedance plot. Ionic conductivity, κ, was calculated using the following expression,

$$\kappa = \frac{L}{aR_b}, [1]$$

where a is electrolyte area calculated using the inner diameter of the spacer, 3.175 mm. The standard deviation was used to estimate error bars from 3 or more cells. Results are reported at 90 °C.

Lithium symmetric cell preparation. Lithium symmetric cells were prepared in a similar manner as the stainless-steel symmetric cells described in the preceding paragraph. Lithium electrodes were constructed by first brushing 150 μm thick lithium metal (MTI Corporation) then pressing using a pneumatic press inside of an argon glovebox to create a clean lithium surface. The lithium metal was backed by nickel foil to increase mechanical support and allow for even current distribution. Electrolytes were heated to 120 °C and pressed into a 3.175 mm diameter hole within a 250 μm thick silicone spacer. Cells were constructed by pressing the lithium electrodes on either side of the silicon spacer containing polymer electrolyte. The electrode thickness was measured using a micrometer. The thickness of each electrolyte (L) was determined by measuring the thickness of the cell and subtracting the thickness of the electrodes. On average, $L = 0.025 \pm 0.01$ cm. Nickel tabs were secured to the nickel side of the electrodes. These cells were vacuum sealed in pouch material leaving the nickel tabs exposed.

Lithium symmetric cell preconditioning. Lithium symmetric cells were annealed at 90 °C in a custom heating stage for 4 h. Cells were preconditioned in order to stabilize the solid electrolyte interface (SEI) before electrochemical characterization at 90 °C using a Biologic VMP3 potentiostat paired with EC Lab software. Preconditioning consisted of five to eight polarization cycles with an applied current density (i) of 0.02 mA cm^{-2} for 4 h in both the positive and negative directions with a 2 h open circuit voltage (OCV) relaxation step between each polarization step. Impedance spectroscopy was performed in between each polarization cycle with a frequency range of 1 MHz to 100 mHz and amplitude of 50 mV. Time independent impedance spectroscopy data were taken as a signature of a stable SEI.

Chronoamperometry. The steady-state current experiment was performed by polarizing preconditioned lithium symmetric cells at constant potential, ΔΦ, for 4 hours and measuring the current density reached at steady-state, i_{SS}. Impedance spectra were collected at every hour increment to probe the bulk and interfacial resistances (R_b, R_i). ΔΦ of 10 mV, -10 mV, 20 mV and -20 mV were utilized to ensure the results were independent of the sign and magnitude of the applied potential. The resistances of the cell initially ($R_{b,0}$ and $R_{i,0}$) and at steady-state ($R_{b,SS}$ and $R_{i,SS}$) were measured using impedance spectroscopy. The initial current density, i_{Ω}, is determined using Ohm's law,

$$i_{\Omega} = \frac{\Delta\Phi}{R_{i,0} + R_{b,0}} \quad .[2]$$

The steady-state current fraction, ρ_+, is calculated as follows,

$$\rho_+ = \frac{i_{ss}(\Delta\Phi - i_{\Omega}R_{i,0})}{i_{\Omega}(\Delta\Phi - i_{ss}R_{i,ss})} \quad .[3]$$

Concentration polarization. Restricted diffusion coefficient measurements were obtained using the concentration polarization introduced by the steady-state current experiment outlined in the preceding paragraph. Upon removal of the applied potential, the open-circuit voltage, *OCV*, of the cell relaxed with time, *t*, for 4 h. The diffusion coefficient, *D*, is calculated as follows

$$\frac{-d\ \ln OCV}{dt} = \frac{\pi^2 D}{L^2}, [4]$$

where the left-hand side of the equation is the slope from the linear fit of –ln(*OCV*) vs. *t*. *L* is the thickness of the electrolyte. The standard deviation was used to estimate error bars from 3 or more cells.

Limiting current density experiments. Current (*i*) was applied to preconditioned lithium symmetric cells containing polymer with a salt concentration of $r = 0.10$ in a stepwise manner, until the limiting current density (i_{lim}) was reached. All experiments were conducted at 90 °C. A cycle for one current experiment consisted of applying the same magnitude of current in the positive direction until the potential reached steady state followed by applying current in the negative direction with 1h open circuit rest steps in between each step. A sample experiment is shown in Figure S1 in the Supporting Information. The time required to reach steady state potential (Φ_{ss}) varied from approximately 25 minutes to 4 h. In most cases, cells were used for one or two current cycles as the nucleation and growth of lithium dendrites short-circuited the cell. Polarization time was minimized to reduce the influence of dendritic growth. Impedance spectroscopy experiments were performed before and after each polarization step to determine the bulk and interfacial impedances.

Concentration cell potential experiments. Concentration cells were prepared by creating a channel with dimensions 4 cm by 1.5 mm in a 250 μm thick silicone. Half of the channel was filled with reference electrolyte with a salt concentration of $r = 0.08$, and the other half was filled with electrolytes at different *r*. Lithium electrodes (lithium foil backed by nickel foil) were placed on both ends of the channel. Nickel tabs were secured to the electrodes. The assembly was vacuum sealed in pouch material. Each cell was annealed at 90 °C for 24 h before the value

of cell potential, U was recorded; this length of time ensures the formation of stable interface layers prior to the electrochemical measurement. The concentration gradient relaxation process was measured over the course of several days. Three concentration cells were prepared at each salt concentration.

Small-angle X-ray scattering.

The morphologies of the electrolytes were determined using small-angle X-ray scattering (SAXS). Samples were prepared inside an argon glovebox. Electrolytes were heated to 120 °C, then pressed into rubber spacers (1 mm thick, 3.175mm inner diameter). Kapton windows were attached to either side of the electrolyte, and the assembly was sealed inside custom airtight aluminum holders. The samples were annealed at 120 °C under vacuum for at least 48 h. Measurements were performed at Beamline 7.3.3. at the Advanced Light Source (ALS) at Lawrence Berkeley National Laboratory and Beamline 1–5 at the Stanford Synchrotron Radiation Lightsource (SSRL) at SLAC National Accelerator Laboratory. Samples were held at 90 °C for at least 30 minutes in a custom-built heating stage before scans were taken. Silver behenate was used to determine the beam center and sample-to-detector distance. Two-dimensional scattering patterns were integrated azimuthally using the Nika program for IGOR Pro to produce one-dimensional scattering profiles.[33] Here we report the scattering intensity as a function of the magnitude of the scattering vector, q ($q = 4\pi sin(\theta/2)/\lambda$) where θ is the scattering angle, and λ is the wavelength of the X-rays equal to 1.2398 Å at the ALS and 1.03232 Å at SSRL.

Results and Discussion.

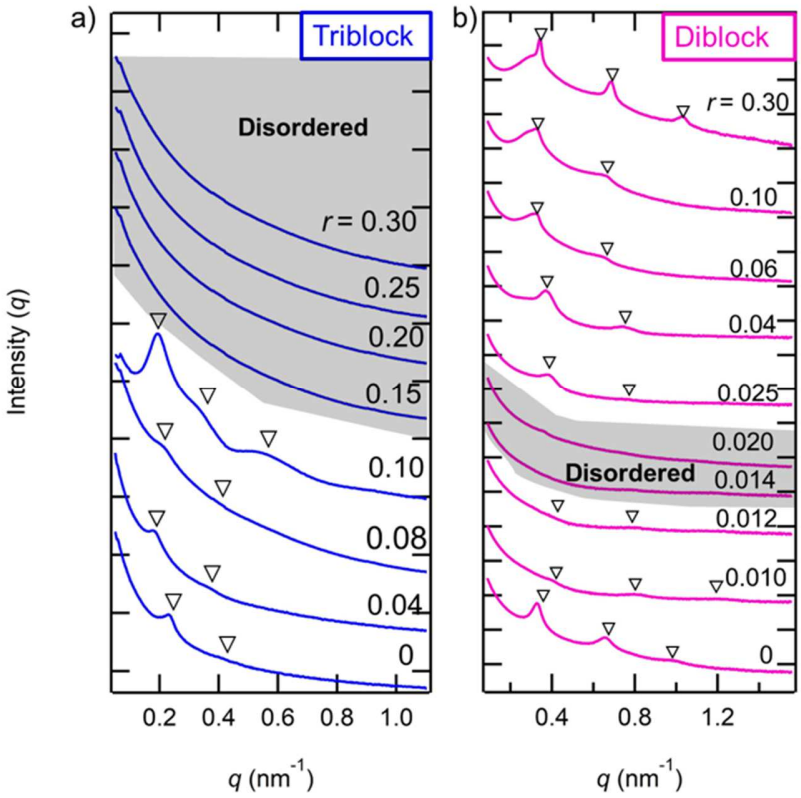

Figure 1. SAXS intensity is plotted as a function of the magnitude of the scattering vector, *q,* in a) triblock and b) diblock copolymer/salt mixtures at 90 °C. Salt concentration, *r*, is indicated on the right ($0 \leq r \leq 0.30$). ▼indicate peaks characteristic of lamellae ($q = q^*, 2q^*, 3q^*$). Shaded gray scans indicate disordered scattering profiles.

The effect of added salt on the morphology is shown in Figure 1a and 1b, where SAXS intensity is plotted as a function of the magnitude of the scattering vector, q at varied salt concentration, [Li]/[EO] = r. Figure 1a shows data for the triblock copolymer/salt mixtures. In the neat sample ($r = 0$), the SAXS pattern exhibits two peaks at $q = q^* = 0.22$ nm^{-1} and $q = 2q^*$, denoted by triangles, indicating the presence of alternating PEO/salt-rich and POSS-rich lamellae layers (*LAM*). The *LAM* morphology persists in the salt concentration range $0 \leq r \leq 0.10$. At $r = 0.15$, we see a monotonically decaying scattering profile, a standard signature of a disordered phase (*DIS*). *DIS* persists in the salt concentration range $0.15 \leq r \leq 0.30$. Thus, a transition from *LAM* to *DIS* occurs with increasing salt concentration at $r = 0.125 \pm 0.025$.

Figure 1b shows SAXS profiles for the diblock copolymer/salt mixtures. At salt concentrations $0 \leq r \leq 0.012$, the SAXS pattern reveals 3 peaks at $q = q^* = 0.35 \pm 0.02$ nm^{-1}, $q = 2q^*$, and $q = 3q^*$, denoted by triangles, indicating *LAM*. At $r = 0.014$, we see a monotonically decaying scattering profile, a standard signature of a disordered phase (*DIS*). *DIS* persists in the salt concentration range $0.014 \leq r \leq 0.02$. At $r \geq 0.025$, a *LAM* phase is observed in the scattering profiles and persists in the accessible salt concentration range ($0.025 \leq r \leq 0.30$). Thus, the diblock copolymer system exhibits a small *DIS* window with a lower boundary at salt concentration $r = 0.013 \pm 0.001$ and an upper boundary at $r = 0.0225 \pm 0.0025$.

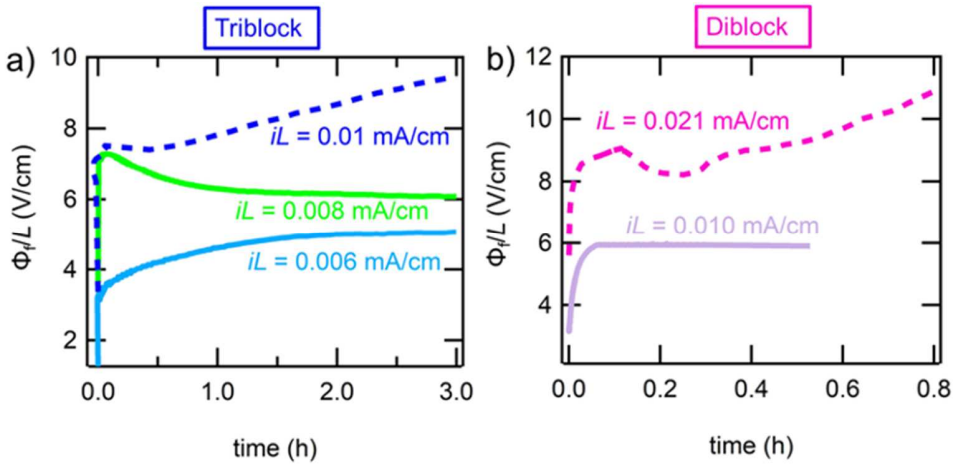

Figure 2. Length-normalized measured cell potential, Φ_f/L versus time for lithium symmetric cells of salt concentration r = 0.1 at different magnitudes of normalized applied current density, iL in a) triblock copolymer and b) diblock copolymer electrolytes at 90 °C. Solid lines indicate profiles where the cell reaches a steady-state potential during polarization current density below the limiting current. Dashes lines indicate profiles where potential diverges due to transport limitations above the limiting current density during polarization at high current density. Figure a) also demonstrates profiles in which an underdamped potential profile is observed at a polarization current density approaching the limiting current. Such profiles are not observed in b).

Figure 2a demonstrates time-dependence of the potential gradient, Φ_f/L, at several applied normalized current densities, iL, in lithium symmetric cells containing the triblock copolymer electrolytes with a salt concentration of r = 0.10. The parameter Φ_f is the potential drop across the cell after correcting for interfacial impedances. It thus accounts for the potential drop across

the bulk electrolyte. The value of Φ_f is obtained after contributions from the interfacial impedance are subtracted according to Ohm's law as follows

$$\Phi_f = \Phi - iR_i a. \quad [5]$$

In a symmetric cell, the dependence of Φ_f obtained at steady state at a given current density, i, will depend on electrolyte thickness, L. We have chosen to display our results on a plot of Φ_f/L versus iL because, in theory, this dependence should be independent of electrolyte thickness. Our choice of parameters used in Figure 2 facilitates comparisons with measurements conducted in other laboratories. The value of interfacial resistance, R_i was obtained by impedance spectra taken in between each current step, and a is electrolyte area calculated using the inner diameter of the spacer used to contain the electrolyte in the lithium symmetric cell (3.175 mm).

At iL = 0.006 mA/cm, Φ_f/L increases with time then reaches a plateau after 2 hours at approximately 5 V/cm. The overdamped time-dependence seen in Figure 2a is a standard signature of a potential profile wherein $i < i_{lim}$. When iL is increased to 0.008 mA/cm, we see a fundamentally different profile. Φ_f/L initially increases with time to a value of 7.5 V/cm. However, over the course of the next 2 hours, Φ_f/L decreases and reaches a plateau at a value of 6 V/cm. In many dynamical systems increasing the magnitude of the perturbation results in a change from overdamped to underdamped behavior.[34] This is true for both linear and nonlinear systems. The result in Figure 2a is thus not surprising, given the highly non-linear nature of ion transport through electrolytic systems, especially as the limiting current is approached.[19,35] The behavior shown in Figures 2a is reversible: decreasing the current density back from iL = 0.008 mA/cm to iL = 0.006 mA/cm results in a return to overdamped dynamics and thus, is not

ascribed to effects such as the unstable deposition of lithium metal on the electrode. At iL = 0.01 mA/cm, Φ_f/L continually increases with time and does not plateau over the course of 4 hours. This is an indication that the limiting current has been exceeded and $i > i_{lim}$. The crossover from overdamped to underdamped behavior appears to be an announcement that the triblock copolymer electrolyte is in the vicinity of the limiting current.

Figure 2b demonstrates Φ_f/L versus time in two lithium symmetric cells containing the diblock copolymer electrolyte with salt concentration r = 0.10 at two different applied currents. At iL = 0.01 mA/cm, a similar overdamped profile to that seen in Figure 2a at iL = 0.006 mA/cm is seen, indicating $i < i_{lim}$. At iL = 0.021 mA/cm, a similar profile to that seen in Figure 2a at iL = 0.010 mA/cm, is seen indicating $i > i_{lim}$. We note that underdamped time-dependence is not seen in any of the diblock copolymer electrolyte potential profiles.

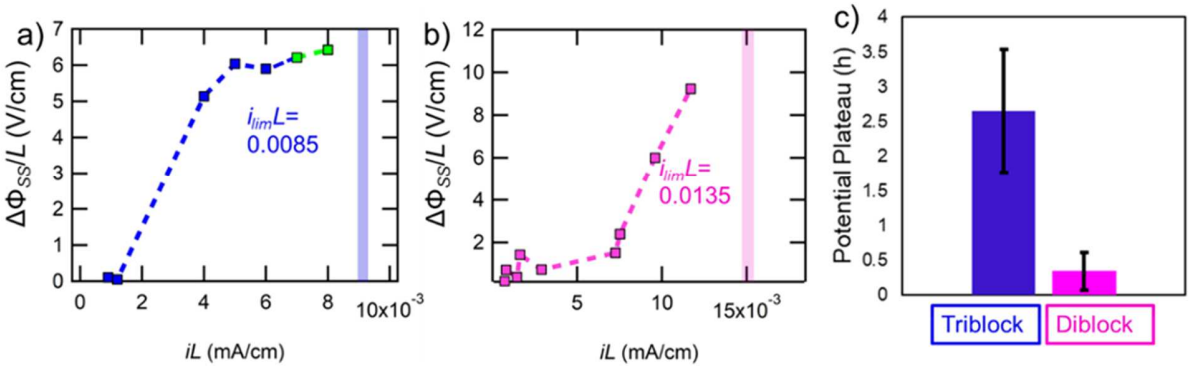

Figure 3. Length-normalized steady-state cell potential, $\Delta\Phi_{SS}/L$, plotted against normalized applied current density, iL, in a) triblock copolymer and b) diblock copolymer electrolytes in lithium symmetric cells of approximate thickness L = 300 μm at salt concentrations r = 0.10 at 90 °C. Each data point represents a unique cell. Horizontal bars indicate measurements where potential diverges due to transport limitations above the limiting current density during polarization. The limiting current density, $i_{lim}L$, is the

average between the last normal measurement, and the horizontal bar. c) Time required to reach the potential plateau averaged across all experiments conducted at currents below the limiting current.

The results of all current density experiments performed on the triblock copolymer electrolyte (r = 0.10) at 90 °C are summarized in Figure 3a where the steady-state potential gradient $\Delta\Phi_{SS}/L$, is plotted as a function of normalized current density, iL. $\Delta\Phi_{SS}$ represents the plateau in potential that is reached in experiments performed at $i < i_{lim}$. $\Delta\Phi_{SS}$ was subtracted by the OCV potential which was slightly greater or less than zero due to the Seebeck effect and unavoidable temperature gradients in the cell. Closed blue data points represent profiles in which an overdamped potential profile is seen (see Figure 2a, iL = 0.006 mA/cm). Green data points represent an underdamped potential profile (see Figure 2a, iL = 0.008 mA/cm). The vertical bar at iL = 0.009 mA/cm indicates $i > i_{lim}$ (see Figure 2a, iL = 0.01 mA/cm). We observe a general increase in $\Delta\Phi_{SS}/L$ with increasing iL. We define the length normalized limiting current, $i_{lim}L$, as the average of the highest current density for which $\Delta\Phi_{SS}$ was observed and the current density at which $\Delta\Phi_{SS}$ was not observed. Thus, $i_{lim}L$ = 0.0085 mA/cm for the triblock copolymer electrolyte. Half of the difference between these two current densities is taken as the error (± 0.0005 mA/cm).

The results of all current density experiments performed on the diblock copolymer electrolyte (r = 0.10) at 90 °C are summarized in Figure 3b. At all current densities classical overdamped potential profiles were observed. As in Figure 3b, the vertical bar at iL = 0.015 indicates $i > i_{lim}$. Using the same method outlined in the preceding paragraph, $i_{lim}L$ = 0.0135 ± 0.0015 mA/cm in the diblock copolymer electrolyte.

Figure 3c plots time to reach plateau potential averaged over all experiments performed in the triblock copolymer (Figure 3a) and the diblock copolymer (Figure 3b) at r = 0.10. The

triblock copolymer electrolytes on average took 2.5 hours to plateau, while the diblock copolymer electrolytes on average took 0.4 hours to plateau. While a rigorous analysis of the time-dependent profiles that underlie the data in Figure 3a and 3b, it is outside of the scope of this paper, a possible reason for this difference will be discussed shortly.

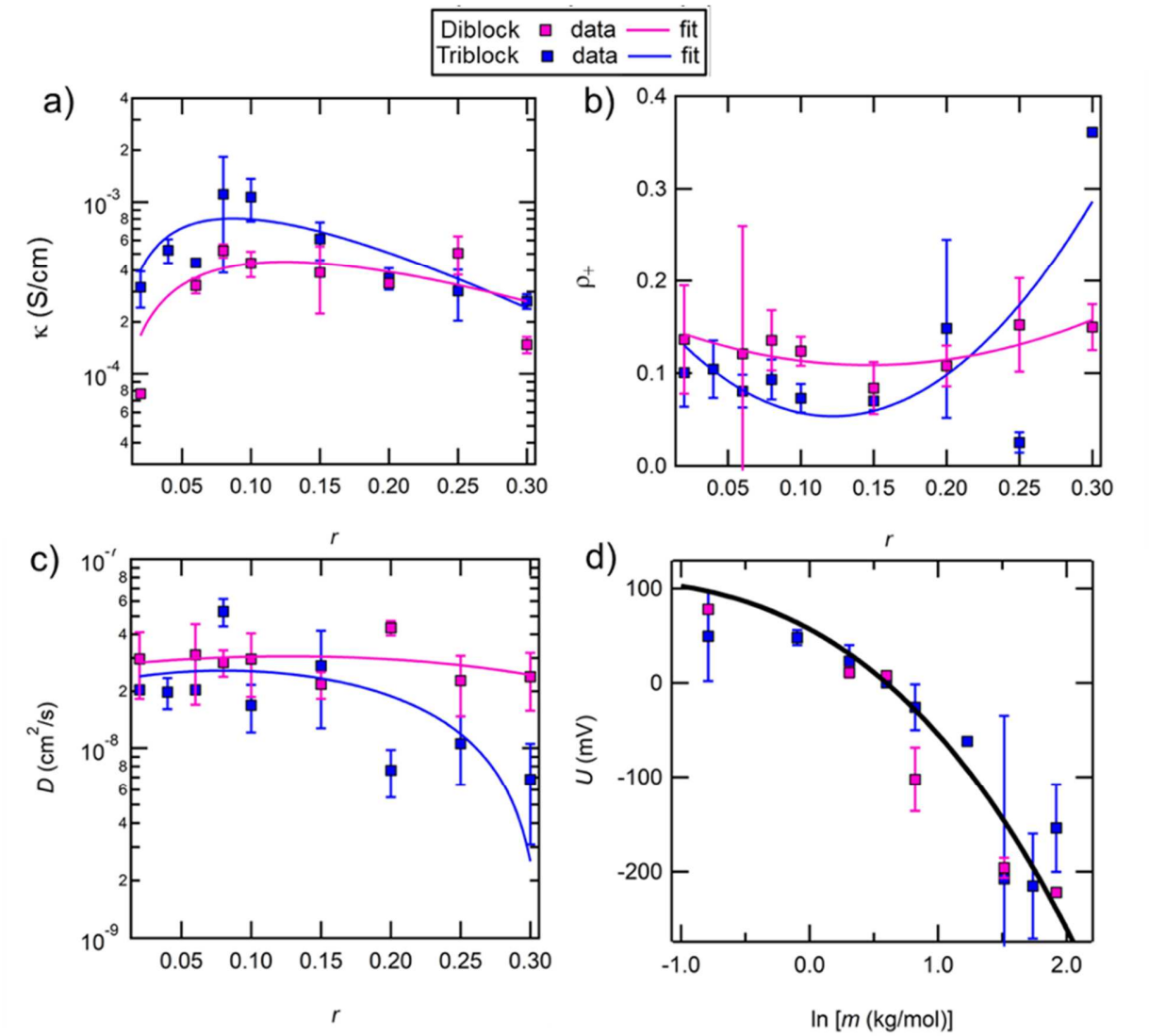

Figure 4. a) Ionic conductivity (κ) b) current fraction (ρ_+) c) diffusion coefficient (D) as a function of salt concentration, r, and d) concentration cell open-circuit potential (U) as a function of natural log molality (ln[m]) at 90 °C. Fits are shown as solid lines through data points.

We use Newman's concentrated solution theory to predict the limiting current in our electrolytes ($i_{lim,th}$) using process described by Pesko *et al*[28]. This requires the full electrochemical characterization of the triblock and diblock copolymer electrolytes at 90 °C, shown in Figure 4a-d.

Figure 4a demonstrates the ionic conductivity (κ) as a function of r at 90 °C shown as markers and fits shown as solid lines to the following expression of the form proposed by Mongcopa *et. al.*[36]

$$\kappa = A_\kappa r_{av} * \exp[-r_{av} / B_\kappa], \quad [6]$$

where A_κ and B_κ are fitting parameters shown in Table 2 for both the diblock and triblock copolymer electrolytes.

Table 2. Fitting parameters used in Figure 4

Diblock	A_x	B_x	C_x
κ	0.0097865	0.12447	--
ρ_+	2.0854	-0.6129	0.1538
D	-2.0534E-07	5.1663E-08	2.7385E-08
U	-13.8	66	74

Triblock	A_x	B_x	C_x
κ	0.025046	0.087231	--
ρ_+	7.2688	1.7677	0.1621

D	-4.8153E-07	7.7335E-08	2.2657E-08
U	-13.8	66	74

Figure 4b demonstrates current fraction (ρ_+) and Figure 4c demonstrates diffusion coefficient (D) as a function of r at 90 °C shown as markers and fits shown as solid lines to the following second-order polynomials

$$\rho_+ = A_{\rho+}\, r_{av}^2 + B_{\rho+}\, r_{av} + C_{\rho+}, \quad [7]$$

$$D = A_D\, r_{av}^{\,2} + B_D\, r_{av} + C_D. \quad [8]$$

where $A_{\rho+}$, $B_{\rho+}$, $C_{\rho+}$, A_D, B_D, and C_D are fitting parameters to the data shown in Figure 4b and 4c for both copolymer electrolytes, shown in Table 2.

The symbols in Figure 4d show the dependence of the concentration cell open-circuit potential (U) on salt molality (m) in the PEO/salt rich microphase. This is calculated assuming all the added salt resides in the PEO-rich microphase. The solid curve in Figure 4d is taken from the work of Galluzzo *et. al.* who studied the open circuit potential in both poly (ethylene oxide) and poly (ethylene oxide)-*b*-poly(styrene) block copolymer electrolytes.[11] That studied compared a wide variety of electrolytes with block copolymer of different molecular weights and compositions and it was found that the open circuit potential from all systems collapsed when plotted as a function of m. This collapse indicates that in block copolymer electrolytes where the salt resides exclusively in one of the domains, the open-circuit potential mainly reflects interactions between the lithium ions and that microphase. It is evident from Figure 4d that the fit that the data obtained by our POSS-containing block copolymers is consistent with the fit presented in ref 7. In this study, we will thus use the parameters given in ref 7.

$$U = A_U \ln[m]^2 + B_U \ln[m] + C_U, \text{ [9]}$$

We note that the concentration cell reference salt concentration used in ref 7 was r_{av} = 0.065. In our experiments, a reference salt concentration used was r = 0.08. A vertical shift was used to adjust the equation used in ref 7 to our data. Our analysis requires evaluation of $\frac{dU}{d\ln[m]}$, which is independent of the vertical shift, and has the following form,

$$\frac{dU}{d\ln[m]} = 2A_U \ln[m] + B_U. \text{ [10]}$$

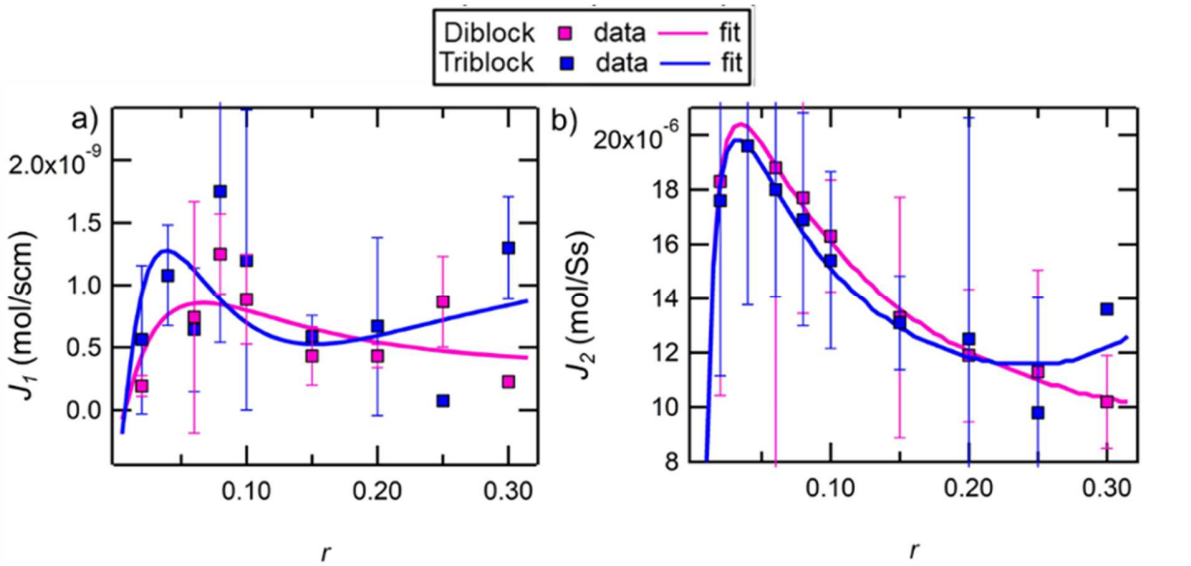

Figure 5. a) J_1 b) J_2 as a function of r at 90 °C in the diblock and triblock copolymer electrolytes. Fits are shown as solid lines through the data.

For a given value of fixed applied current density, i, the salt concentration as a function of position in the cell, $r_{sp}(x)$, is given by the following expression derived in ref 21,

$$\int_{r_{sp}(x=0)}^{r_{sp}(x)} \frac{\kappa(r)[\frac{dU}{d\ln[m]}(r)]}{r(z_+ v_+) f_{EO/LiTFSI}(1-\frac{1}{\rho_+(r)})} dr = \int_{r_{sp}(x=0)}^{r_{sp}(x)} J_1 dr = -iL\,(x/L)\,, [11]$$

where z_+ is the charge number and v_+ is the number of cations. Both z_+ and v_+ equal to 1 for LiTFSI. The integrand in the left side of Equation 11 is called J_1. Our objective is to determine $r_{sp}(x)$ for a given value of average salt concentration, r_{av} and iL. This is done by first guessing $r_{sp}(x = 0)$ and solving for $r_{sp}(x)$ using Equation 11 between $0 \leq x/L \leq 1$ by numerical integration. The average of all calculated $r_{sp}(x)$ for all positions within the cell is then calculated. If it does not agree with the specified value of r_{av}, then $r_{sp}(x = 0)$ is changed until convergence. Once all $r_{sp}(x)$ at different points within the electrolyte are known, then the spatially dependent steady-state potential, $\Phi_{SS}(x)$, can be calculated using the following expression,

$$\Phi_{SS}(x) = \int_{r_{sp}(x=L)}^{r_{sp}(x)} \frac{1}{\kappa(r)\rho_+(r)} J_1 dr, [12]$$

rearranged as follows,

$$\Phi_{SS}(x) = \int_{r_{sp}(x=L)}^{r_{sp}(x)} \frac{\frac{dU}{d\ln[m]}(r)}{r(\rho_+(r)-1)(z_+ v_+) f_{EO/LiTFSI}} dr = \int_{r_{sp}(x=L)}^{r_{sp}(x)} J_2 dr\,. [13]$$

where J_2 is the integrand in Equation 13, analogous to J_1. Without any loss of generality, the potential at $x = L$ is defined to be zero in Equation 13.

The integrands J_1 and J_2 are plotted as a function of r in Figures 5a and 5b. The fitted equation to the data in Figure 4a used to compute the right side of Equation 11 is

$$J_1 = A_1 r\, Exp\left[-\frac{r}{B_1}\right](C_1 r^2 + D_1 r + E_1). \quad [14]$$

The fitted equation to the data in Figure 4b used to compute the right side of Equation 13 is

$$J_2 = A_2 r\, Exp\left[-\frac{r}{B_2}\right](C_2 r^2 + D_2 r + E_2). \quad [15]$$

Table 3. Fitting parameters used in Figure 4.

Triblock	A_x	B_x	C_x	D_x	E_x
1	-0.017759 ± 281	0.086436 ± 0.00341	-0.00015541 ± 2.46	4.3448e-005 ± 0.687	-4.1163e-006 ± 0.0651
2	0.015181 ± 42	0.077453 ± 0.00575	2.7411 ± 7.58e+003	-0.66356 ± 1.84e+003	0.075376 ± 208
Diblock	A_x	B_x	C_x	D_x	E_x
1	5.0738e-006 ± 0.000155	0.11973 ± 0.0122	0.078773 ± 2.4	-0.032477 ± 0.991	0.0061345 ± 0.187
2	0.018888 ± 60.6	0.071005 ± 0.0053	2.3706 ± 7.6e+003	-0.52126 ± 1.67e+003	0.063286 ± 203

All fitting parameters for the fits demonstrated in Figure 5a and 5b using Equations 14 and 15 are shown in Table 3 for both copolymer electrolytes. The fits are extrapolated in the salt concentration range $0 \leq r \leq 0.02$, which lies outside of the range of electrochemical measurements. We note that Equation 14 and 15 have the same form, but different fitted parameters (*A*-*E*). The required integrations were performed analytically using Equations 16 and 17:

$$\int_{r_{sp}(x=0)}^{r_{sp}(x)} J_1 dr = -(A_1B_1\{6B_1^3C_1 + 2B_1^2(D_1 + 3C_1r) + r\,[E_1 + r\,(D_1 + C_1r)]\} + B_1\,[E_1 + r\,(2D_1 + 3C_1r)]\,Exp[-r/B_1]\,|_{r_{sp}(x=0)}^{r_{sp}(x)}. \quad [16]$$

$$\int_{r_{sp}(x=0)}^{r_{sp}(x)} J_2 dr = -(A_2B_2\{6B_2^3C_2 + 2B_2^2(D_2 + 3C_2r + r\,[E_2 + r\,(D_2 + C_2r)]\} + B_2\,[E_2 + r\,(2D_2 + 3C_2r)]\,Exp[-r/B_2]\,|_{r_{sp}(x=0)}^{r_{sp}(x)}. \quad [17]$$

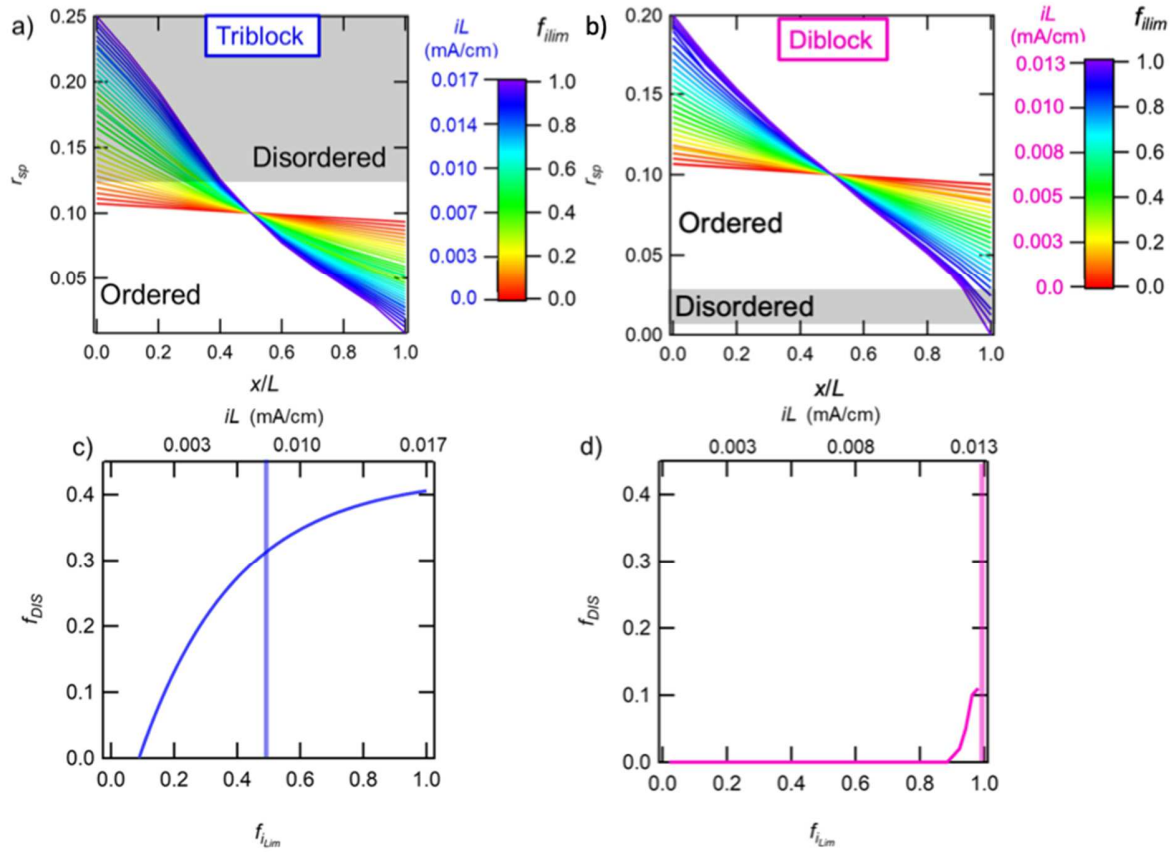

Figure 6. Salt concentration profiles $r_{sp}(x/L)$ as functions of position through the cell at a range of current densities, i, with average salt concentration r_{av} = 0.10 in a) triblock copolymer and b) diblock copolymer electrolytes. x/L = 1 is the cathode side of the cell; x/L = 0 is the anode side of the cell. Fraction of disordered morphology, f_{DIS}, as a function of fraction of theoretical limiting current f_{ilim} in c) triblock copolymer and d) diblock copolymer electrolytes.

Figure 6a and 6b plot the spatially determined salt concentration, r_{sp}, as a function of position ($0 \leq x/L \leq 1$), calculated using Equation 11, for both electrolytes with average salt concentration, r_{av} = 0.10. x/L = 1 is the electrolyte/cathode interface; x/L = 0 is the electrolyte/anode interface. The current density, i, is incrementally increased until the theoretical

limiting current density, $i_{lim,th}$ is reached, (i.e r_{sp} = 0 at x/L = 1). We define a fraction of theoretical limiting current density as follows: $f_{ilim} = i/i_{lim.th}$. The color of each salt concentration gradient corresponds to different values of f_{ilim} and iL. We observe an increase in the salt concentration gradient with increasing f_{ilim} in both electrolytes. $i_{lim,th}$ in the triblock copolymer electrolyte is 0.017 mA/cm, while $i_{lim,th}$ in the diblock copolymer electrolyte is 0.013 mA/cm. We note that the data in the salt concentration range $0 \leq r_{av} < 0.02$ is outside of the range of experimentally determined electrochemical transport parameters and thus is an estimated based upon the fit demonstrated in Figure 5a.

The *DIS* salt concentration window is shaded in gray in Figure 6c and 6b. As shown in Figure 5a and 5b, the *DIS* phase occurs at a larger range of salt concentrations in the triblock copolymer electrolytes as compared to the diblock copolymer electrolytes. The fraction of *DIS*, f_{DIS} is defined as the fraction of electrolyte in the salt concentration range that exhibits *DIS* morphology. Figure 6c and 6d plot f_{ilim} as a function of fraction of f_{DIS} in the triblock copolymer and diblock copolymer electrolyte respectively, where the secondary x-axis plots the corresponding value of iL. The triblock copolymer electrolyte exhibits a steep increase in f_{DIS} at $f_{ilim} > 0.10$. At $f_{ilim} = 1$, f_{DIS} reaches a maximum of 0.40. Figure 6d demonstrates f_{DIS} is much lower in the diblock copolymer electrolyte at all f_{ilim}. f_{DIS} is 0, with the exception of $0.9 < f_{ilim} < 1.0$, where f_{DIS} reaches a maximum of 0.10. Experimentally determined i_{lim} is plotted alongside the data in Figures 6b and 6d, shown as a vertical bar. Figure 6b demonstrates that the triblock copolymer electrolyte i_{lim} is reached when $f_{ilim} = 0.46$, while Figure 6d shows the diblock copolymer electrolyte i_{lim} is reached when $f_{ilim} = 1$. This large difference is attributed to $f_{DIS} = 0.30$ in the triblock copolymer electrolyte, while $f_{DIS} = 0.10$ in the diblock copolymer electrolyte.

The results shown in Figure 6a-d demonstrate that morphology is an important parameter in determining i_{lim}. The model used to estimate the limiting current density does not account for changes in morphology.

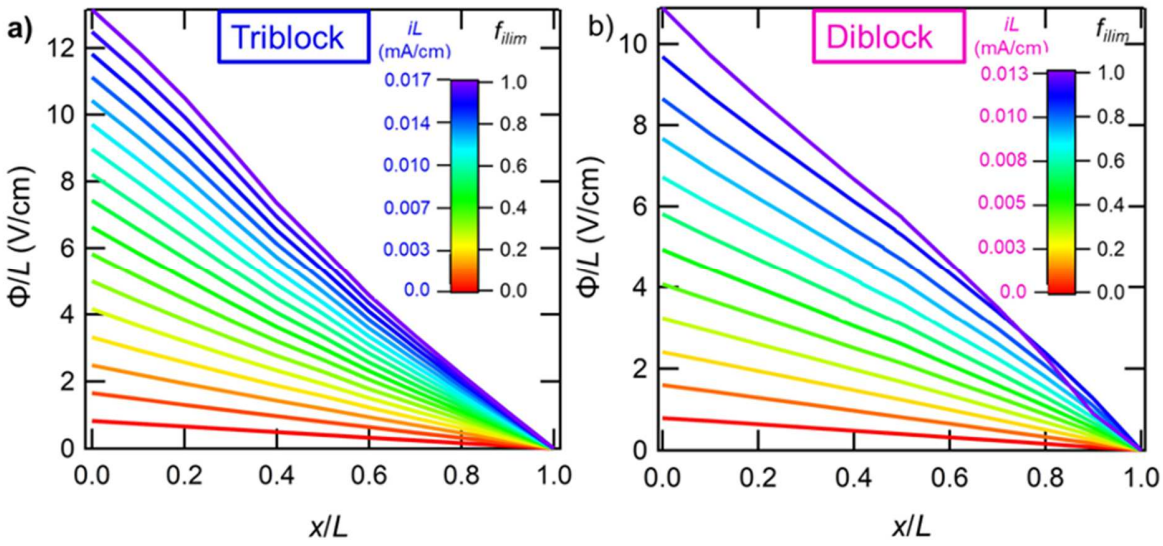

Figure 7. a) Simulated spatially dependent potential normalized by cell thickness (Φ/L) as a function of position in cell (x/L) for a range of r calculated at various current densities, iL in a) triblock copolymer and b) diblock copolymer electrolytes with average salt concentration r = 0.10. The potential at $x = L$ is zero by definition.

Figure 7a and 7b demonstrates the potential normalized by cell thickness (Φ/L) as a function of position in electrolyte (x/L) calculated using Equation 13 in the triblock and diblock copolymer electrolytes respectively. The applied currents are the same as those shown in Figure 6 and range from $0 < i < i_{lim,th}$. The color scale bar notes the corresponding values of iL and f_{ilim}. As in Figure 6a and 6b, the results of the triblock and diblock copolymer simulations are

comparable. The magnitude of Φ/L at $x/L = 0$ is greater in the triblock copolymer electrolytes as compared to the diblock copolymer electrolytes.

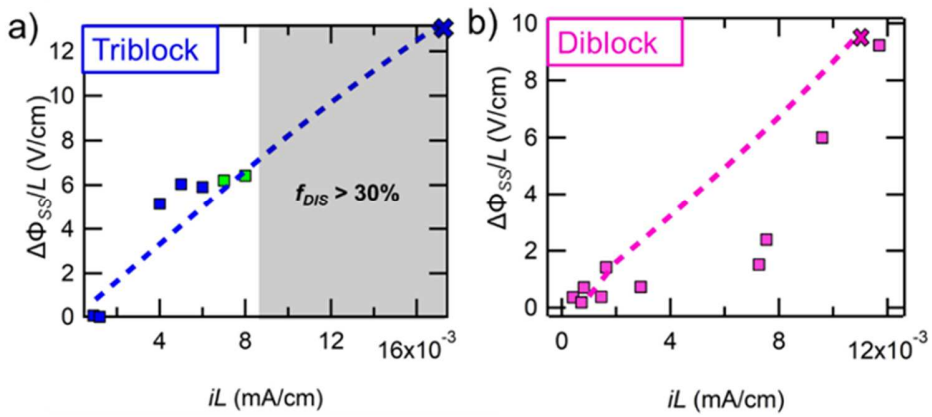

Figure 8. A comparison of experimentally measured (markers) (Figure 2) and theoretically predicted steady-state potential drop (dashed line), $\Delta\Phi_{SS}/L$, versus applied current density, iL normalized by thickness in a) triblock copolymer and b) diblock copolymer electrolytes with $r_{av} = 0.10$. "X" indicates the experimentally determined limiting current. The area shaded in gray indicates where salt concentration profiles indicate that $f_{DIS} > 0.30$.

The theoretically predicted Φ_{SS} is taken to be the value of Φ at $x/L = 0$ and $iL < i_{lim}L$. The dashed curve in Figure 8 shows the theoretically predicted $\Delta\Phi_{SS}/L$. The terminus of this curve, represented by an 'x', represents the theoretical prediction for the limiting current. The data points represent the experimentally measured $\Delta\Phi_{SS}/L$ versus iL, recast from Figure 3a and 3b for the triblock and diblock copolymer electrolytes respectively at $r_{av} = 0.10$.

Figure 8a shows results for the triblock copolymer electrolyte and demonstrates quantitative agreement between experimental and theoretical $\Delta\Phi_{SS}/L$ when $iL < 0.009$ mA/cm. When $iL > 0.009$ mA/cm, the theoretical model predicts a continued linear increase in measured

$\Delta\Phi_{SS}/L$. Experimentally, $iL > 0.009$ mA/cm $> i_{lim}L$. As previously discussed, the measured $i_{lim}L$ is 46% of the theoretical $i_{lim}L$. The shaded regions show the limit $f_{DIS} > 0.30$.

Figure 8b shows the results for diblock copolymer electrolyte and demonstrates lower measured $\Delta\Phi_{SS}/L$ than theoretically predicted $0 < iL < 0.008$ mA/cm. There is better quantitative agreement between experimental and theoretical $\Delta\Phi_{SS}/L$ when $iL > 0.010$. As previously discussed, the measured $i_{lim}L$ (0.0135 ± 0.015) is within error of theoretically predicted $i_{lim}L$ (0.013 mA/cm).

The mismatch between theoretical predictions and our experiments in Figure 8 indicates the need to developing more complete theoretical models for ion transport through nanostructured block copolymers; the approach that we have used based on three transport coefficients and one thermodynamic factor was, after all, developed for homogeneous, single-phase electrolytes[19].

Conclusion.

The limiting current density in symmetric lithium cells at 90°C was determined experimentally in hybrid inorganic-organic triblock and diblock copolymer electrolytes. The time-dependence of the cell potential was recorded at fixed applied current densities. The steady-state cell potential was a smooth function of current density until a threshold; this threshold was taken as an indication that the applied current exceeded the limiting current density. While the diblock copolymer electrolytes exhibited overdamped profiles similar to those in homopolymer PEO, the triblock copolymer exhibited underdamped profiles at applied current densities close to the limiting current.

The diblock and triblock copolymer electrolytes were fully characterized at a large range of salt concentrations using electrochemical methods to determine the ionic conductivity, salt diffusion coefficient, current fraction, and the concentration cell steady-state potential as a function of average salt concentration. Newman's concentrated solution theory was used to simulate cell potential and salt concentration profiles to determine a theoretical limiting current (*i.e.,* the current at which the simulation predicted that the salt concentration at the cathode equals zero). The predicted limiting current is a factor of 2 greater than the experimentally determined limiting current in the triblock copolymer electrolyte. While the diblock copolymer electrolyte remains more-or-less ordered in the accessible salt concentration range, the triblock copolymer electrolyte exhibits a large disordered window at high salt concentrations. Further work must be performed to better theoretically predict limiting current in complex, multicomponent systems.

Author Contributions.

The manuscript was written through contributions of all authors. All authors have given approval to the final version of the manuscript.

Notes.

The authors declare no competing financial interest.

Acknowledgement.

This work was supported by the Assistant Secretary for Energy Efficiency and Renewable Energy, Office of Vehicle Technologies of the U.S. Department of Energy under Contract DE-

AC02-05CH11231 under the Battery Materials Research Program. X-ray work performed at Advanced Light Source, which is a DOE Office of Science User Facility, was supported by Contract No. DE-AC02- 05CH11231. X-ray work performed at the Stanford Synchrotron Radiation Light Source, a user facility at SLAC National Accelerator Laboratory, was supported by the U.S. Department of Energy, Office of Science, Office of Basic Energy Sciences under Contract No. DE-AC02-76SF00515. Work at the Molecular Foundry was supported by the Office of Science, Office of Basic Energy Sciences, of the U.S. Department of Energy under Contract No. DE-AC02-05CH11231. G.K.S. acknowledges funding from a National Science Foundation Graduate Student Research Fellowship.

LIST OF SYMBOLS

a	electrolyte area (cm^2)
A_κ	ionic conductivity versus salt concentration expression prefactor
$A_{\rho+}$	first fitting parameter cation current fraction versus salt concentration expression
A_D	first fitting parameter salt diffusion coefficient versus salt concentration expression
A_U	first fitting parameter open circuit potential versus salt concentration expression
B_κ	ionic conductivity versus salt concentration expression exponential factor
$B_{\rho+}$	second fitting parameter cation current fraction versus salt concentration expression
B_D	second fitting parameter salt diffusion coefficient versus salt concentration expression

B_U	second fitting parameter open circuit potential versus salt concentration expression
$C_{\rho+}$	third fitting parameter cation current fraction versus salt concentration expression
C_D	third fitting parameter salt diffusion coefficient versus salt concentration expression
C_U	third fitting parameter open circuit potential versus salt concentration expression
d	domain spacing (nm) at 90 °C
D	salt diffusion coefficient (cm/s)
f_{DIS}	fraction of disordered phase
f_{EO}	volume fraction of the PEO block
$f_{EO/LiTFSI}$	volume fraction of the PEO/LiTFSI-rich block
f_{ilim}	fraction of current density to theoretical limiting current density
i	current density (mA/cm^2)
i_{lim}	limiting current density (mA/cm^2)
$i_{lim,th}$	theoretical limiting current density (mA/cm^2)
J_1	integrand expression for spatially determined salt concentration expression
J_2	integrand expression for spatially dependent steady-state potential
L	thickness of the electrolyte (cm)
m	molality (mol/kg)
M_{PEO}	molecular weight of the PEO block (kg/mol)
M_{POSS}	molecular weight of the POSS block (kg/mol)
N	chain length calculated at 120 °C and monomer reference volume of 0.1 nm^3
q	magnitude of scattering vector (nm^{-1})

q^*	magnitude of scattering vector at the primary scattering peak (nm^{-1})
r	salt concentration equal to the ratio of lithium to ethylene oxide moieties
r_{av}	average electrolyte ratio of lithium to ethylene oxide moieties
r_{sp}	spatially determined ratio of lithium to ethylene oxide moieties
R_i	interfacial resistance (Ω)
U	concentration cell open circuit potential (V)
v_+	number of cations in salt
x	position in electrolyte (cm)
z_+	charge number of cation

GREEK

κ	ionic conductivity (S/cm^2)
ρ_+	cation current fraction
Φ	cell potential (V)
Φ_f	cell potential corrected for interfacial impedances (V)
$\Delta\Phi_{ss}$	steady-state potential (V)
θ	SAXS scattering angle
λ	SAXS wavelength (nm)

References

1. Armand, M. & Tarascon, J. M. Building better batteries. *Nature* **451,** 652–657 (2008).

2. Ryou, M. H., Lee, D. J., Lee, J. N., Lee, Y. M., Park, J. K. & Choi, J. W. Excellent cycle

life of lithium-metal anodes in lithium-ion batteries with mussel-inspired polydopamine-coated separators. *Adv. Energy Mater.* **2,** 645–650 (2012).

3. Wood, K. N., Noked, M. & Dasgupta, N. P. Lithium metal anodes: Toward an improved understanding of coupled morphological, electrochemical, and mechanical behavior. *ACS Energy Lett.* **2,** 664–672 (2017).
4. Mindemark, J., Lacey, M. J., Bowden, T. & Brandell, D. Beyond PEO—Alternative host materials for Li+-conducting solid polymer electrolytes. *Prog. Polym. Sci.* **81,** 114–143 (2018).
5. Panday, A., Mullin, S., Gomez, E. D., Wanakule, N., Chen, V. L., Hexemer, A., Pople, J. & Balsara, N. P. Effect of molecular weight and salt concentration on conductivity of block copolymer electrolytes. *Macromolecules* **42,** 4632–4637 (2009).
6. Ehrl, A., Landesfeind, J., Wall, W. A. & Gasteiger, H. A. Determination of Transport Parameters in Liquid Binary Lithium Ion Battery Electrolytes. *J. Electrochem. Soc.* **164,** A826–A836 (2017).
7. Bazak, J. D., Allen, J. P., Krachkovskiy, S. A. & Goward, G. R. Mapping of Lithium-Ion Battery Electrolyte Transport Properties and Limiting Currents with In Situ MRI. *J. Electrochem. Soc.* **167,** 140518 (2020).
8. Bouridah, A., Dalard, F., Deroo, D. & Armand, M. B. Potentiometric measurements of ionic transport parameters in poly(ethylene oxide)-LiX electrolytes. *J. Appl. Electrochem.* **17,** 625–634 (1987).
9. Edman, L., Doeff, M. M., Ferry, A., Kerr, J. & De Jonghe, L. C. Transport properties of the solid polymer electrolyte system P(EO)nLiTFSI. *J. Phys. Chem. B* **104,** 3476–3480 (2000).

10. Ravn Sorensen, P. & Jacobsen, T. Limiting Current in the Polymer Electrolyte: PEOxLICF3SO 3. *Solid State Ionics* **6,** 1147–1154 (1983).

11. Galluzzo, M. D., Loo, W. S., Wang, A. A., Walton, A., Maslyn, J. A. & Balsara, N. P. Measurement of Three Transport Coefficients and the Thermodynamic Factor in Block Copolymer Electrolytes with Different Morphologies. *J. Phys. Chem. B* **124,** 921–935 (2020).

12. Shang, D., Fu, J., Lu, Q., Chen, L., Yin, J., Dong, X., Xu, Y., Jia, R., Yuan, S., Chen, Y. & Deng, W. A novel polyhedral oligomeric silsesquioxane based ionic liquids (POSS-ILs) polymer electrolytes for lithium ion batteries. *Solid State Ionics* **319,** 247–255 (2018).

13. Fu, J., Lu, Q., Shang, D., Chen, L., Jiang, Y., Xu, Y., Yin, J., Dong, X., Deng, W. & Yuan, S. A novel room temperature POSS ionic liquid-based solid polymer electrolyte. *J. Mater. Sci.* **53,** 8420–8435 (2018).

14. Elsøe, K., Kraglund, M. R., Grahl-Madsen, L., Scherer, G. G., Hjelm, J., Jensen, S. H., Jacobsen, T. & Mogensen, M. B. Noise Phenomena in Electrochemical Impedance Spectroscopy of Polymer Electrolyte Membrane Electrolysis Cells. *Fuel Cells* **18,** 640–648 (2018).

15. Bruce, P. G., Hardgrave, M. T. & Vincent, C. A. The determination of transference numbers in solid polymer electrolytes using the Hittorf method. *Solid State Ionics* **53–56,** 1087–1094 (1992).

16. Andrews, S., Evans, J., Vincent, C. A. & Bruce, P. G. Electrochemical measurement of transference numbers in polymer electrolytes. *Polymer (Guildf).* **28,** 2324–2328 (1987).

17. Ma, Y., Doyle, M., Fuller, T. F., Doeff, M. M., De Jonghe, L. C. & Newman, J. The Measurement of a Complete Set of Transport Properties for a Concentrated Solid Polymer

Electrolyte Solution. *J. Electrochem. Soc.* **142,** 1859–1868 (1995).

18. Um, S. & Wang, C. Y. Three-dimensional analysis of transport and electrochemical reactions in polymer electrolyte fuel cells. *J. Power Sources* **125,** 40–51 (2004).
19. Newman, J. & Balsara, N. P. *Electrochemical Systems*. (John Wiley & Sons, Ltd, 2021).
20. Chang, H. J., Ilott, A. J., Trease, N. M., Mohammadi, M., Jerschow, A. & Grey, C. P. Correlating Microstructural Lithium Metal Growth with Electrolyte Salt Depletion in Lithium Batteries Using 7 Li MRI. *J. Am. Chem. Soc.* **137,** 15209–15216 (2015).
21. Frenck, L., Sethi, G. K., Maslyn, J. A. & Balsara, N. P. Factors That Control the Formation of Dendrites and Other Morphologies on Lithium Metal Anodes. *Front. Energy Res.* **7,** (2019).
22. Sethi, G. K., Jiang, X., Chakraborty, R., Loo, W. S., Villaluenga, I. & Balsara, N. P. Anomalous Self-Assembly and Ion Transport in Nanostructured Organic–Inorganic Solid Electrolytes. *ACS Macro Lett.* 1056–1061 (2018). doi:10.1021/acsmacrolett.8b00583
23. Sethi, G. K., Jung, H. Y., Loo, W. S., Sawhney, S., Park, M. J., Balsara, N. P. & Villaluenga, I. Structure and Thermodynamics of Hybrid Organic–Inorganic Diblock Copolymers with Salt. *Macromolecules* acs.macromol.9b00042 (2019). doi:10.1021/acs.macromol.9b00042
24. Loo, W. S., Galluzzo, M. D., Li, X., Maslyn, J. A., Oh, H. J., Mongcopa, K. I. S., Zhu, C., Wang, A. A., Wang, X., Garetz, B. A. & Balsara, N. P. Phase Behavior of Mixtures of Block Copolymers and a Lithium Salt. *J. Phys. Chem. B* **122,** acs.jpcb.8b04189 (2018).
25. Sethi, G. K., Chakraborty, S., Zhu, C., Schaible, E., Villaluenga, I. & Balsara, N. P. Effect of crystallization of the polyhedral oligomeric silsesquioxane block on self-assembly in hybrid organic-inorganic block copolymers with salt. *Giant* **6,** 100055 (2021).

26. Shah, D. B., Kim, H. K., Nguyen, H. Q., Srinivasan, V. & Balsara, N. P. Comparing Measurements of Limiting Current of Electrolytes with Theoretical Predictions up to the Solubility Limit. *J. Phys. Chem. C* **123,** 23872–23881 (2019).

27. Gribble, D. A., Frenck, L., Shah, D. B., Maslyn, J. A., Loo, W. S., Mongcopa, K. I. S., Pesko, D. M. & Balsara, N. P. Comparing Experimental Measurements of Limiting Current in Polymer Electrolytes with Theoretical Predictions. *J. Electrochem. Soc.* **166,** A3228–A3234 (2019).

28. Pesko, D. M., Feng, Z., Sawhney, S., Newman, J., Srinivasan, V., Balsara, N. P. & Berkeley, L. Comparing Cycling Characteristics of Symmetric Lithium-Polymer-Lithium Cells with Theoretical Predictions. *J. Electrochem. Soc.* **165,** 3186–3194 (2018).

29. Frenck, L., Veeraraghavan, V. D., Maslyn, J. A., Müller, A., Ho, A. S., Loo, W. S., Minor, A. M. & Balsara, N. P. Effect of salt concentration profiles on protrusion growth in lithium-polymer-lithium cells. *Solid State Ionics* **358,** (2020).

30. Park, J. W., Yoshida, K., Tachikawa, N., Dokko, K. & Watanabe, M. Limiting current density in bis(trifluoromethylsulfonyl)amide-based ionic liquid for lithium batteries. *J. Power Sources* **196,** 2264–2268 (2011).

31. Lee, S. I., Jung, U. H., Kim, Y. S., Kim, M. H., Ahn, D. J. & Chun, H. S. A study of electrochemical kinetics of lithium ion in organic electrolytes. *Korean J. Chem. Eng.* **19,** 638–644 (2002).

32. Georén, P. & Lindbergh, G. Characterisation and modelling of the transport properties in lithium battery polymer electrolytes. *Electrochim. Acta* **47,** 577–587 (2001).

33. Ilavsky, J. Nika: Software for two-dimensional data reduction. *J. Appl. Crystallogr.* **45,** 324–328 (2012).

34. Bequette, B. *Process control: modeling, design, and simulation*. (2003).

35. Ugata, Y., Thomas, M. L., Mandai, T., Ueno, K., Dokko, K. & Watanabe, M. Li-ion hopping conduction in highly concentrated lithium bis(fluorosulfonyl)amide/dinitrile liquid electrolytes. *Phys. Chem. Chem. Phys.* **21,** 9759–9768 (2019).

36. Mongcopa, K. I. S., Tyagi, M., Mailoa, J. P., Samsonidze, G., Kozinsky, B., Mullin, S. A., Gribble, D. A., Watanabe, H. & Balsara, N. P. Relationship between Segmental Dynamics Measured by Quasi-Elastic Neutron Scattering and Conductivity in Polymer Electrolytes. *ACS Macro Lett.* **7,** 504–508 (2018).